 CMC, vol.18, no.3, pp.271-299, 2010

Efficiency of Power Dissipation and Instability Criterion for Processing Maps in Hot Forming

J. Luo[1] **and M.Q. Li**[1,2]

Abstract: The processing maps are a superimposition of iso-efficiency contour map and flow instability map, which are used to design hot working processing conditions in a wide variety of materials. In order to construct the processing maps, the efficiency of power dissipation and an instability criterion taking into account the contribution of strain and microstructure evolution are proposed based on a set of microstructure-based viscoplastic constitutive equations. In viscoplastic constitutive equations, the grain size of matrix phase and the dislocation density are taken as internal state variables. And, the material constants in present equations can be identified by a genetic algorithm (GA)-based objective optimization technique. Isothermal compression of Ti-6Al-4V alloy is conducted on a Thermecmaster-Z simulator with different deformation temperatures, strain rates and height reductions so as to establish the processing maps by using the present model. The primary α grain size is measured at an OLYMPUS PMG3 microscope with the quantitative metallography image analysis software. Based on the experimental results, the processing maps of Ti-6Al-4V alloy are constructed at different strains. The processing maps show that the instability domains and the efficiency of power dissipation vary as the strain increases. The comparison between the processing maps of present study and that based on Prasad's theory shows that the present processing maps can more efficiently describe the deformation behavior and provide more appropriately physical interpretation and optimize processing conditions accurately.

Keywords: Efficiency of power dissipation; Instability criterion; Titanium alloy; Constitutive equation; Grain size

[1] School of Materials Science and Engineering, Northwestern Polytechnical University, Xi'an 710072, P.R. China

[2] Corresponding author, Tel. +86 29 88491478, E-mail: honeymli@nwpu.edu.cn

1 Introduction

Metal forming are used not only to impose the required shape change, but also to impart the desired microstructure change in the material. During practical metal-working processes, flow localization generally occurs under complex conditions of loading and deformation, but the source of flow localization is often difficult to pinpoint or quantify. As a result, the methods of avoiding such occurrences are often selected on the basis of a trial-and-error procedure or on experience-based judgments [Semiatin (1984)]. However, these methods, which are expensive and time consuming, may not always be a successful solution or optimization. In the past two decades, processing modeling is developed and widely used to forecast the extent of plastic deformation to prevent the occurrences of flow localization or fracture. One of the modeling approaches, such as deformation mechanism maps, is defined to delineate 'safe' and 'non-safe' processing conditions. These deformation mechanism maps show the processing conditions for stable and unstable deformation [Narayana Murty, Torizuka and Nagai (2005)].

Frost and Ashby (1982) attempted firstly to establish the materials response in the form of deformation mechanism map in which the emphasis has been essentially on the creep mechanisms applicable to lower strain rates. Raj (1981) extended the concept of Ashby's maps so as to establish a processing map on the basis of cavity nucleation mechanisms, dynamic recrystallization and adiabatic heating effects. The map represents the limiting conditions for cavity formation at hard particles in a soft matrix occurring at lower temperatures and higher strain rates, and wedge cracking at grain boundary triple junctions occurring at higher temperatures and lower strain rates. Semiatin and Lahoti (1981, 1982) proposed a correlation between the occurrence of shear bands and the flow localization parameter α ($\alpha = -\gamma/m$, where γ is the normalized flow softening rate in compression, m is the strain rate sensitivity exponent) during plane-strain deformation. Subsequently, the processing maps which were used to design hot working schedules for making near-net shapes in a wide variety of materials were established on the basis of dynamic materials modeling (DMM) [Prasad, Gegel, Doraivelu, Malas, Morgan, Lark and Barker (1984); Prasad and Rao (2005, 2006, 2008); Prasad, Rao, Hort and Kainer (2008); Prasad, Sasidhara and Sikka (2000); Prasad, Sastry and Deevi (2000, 2001); Prasad and Seshacharyulu (1998); Seshacharyulu, Medeiros, Frazier and Prasad (2000, 2001, 2002); Seshacharyulu, Medeiros, Morgan, Malas, Frazier and Prasad (2000)]. This approach was reviewed by Gegel, Malas, Doraivelu and Shende (1988) and Alexander (1989). According to the DMM, the dissipation co-content J is given by $J = \int_0^\sigma \dot{\varepsilon} d\sigma = \frac{\sigma \dot{\varepsilon} m}{m+1}$ and the efficiency of power dissipation η is written as $\eta = \frac{J}{J_{\max}} = \frac{2m}{m+1}$ when the flow stress obeys power law $\sigma = K\dot{\varepsilon}^m$, where K is the material constant, σ is the flow stress (MPa), and $\dot{\varepsilon}$ is the strain rate

(s^{-1}). The optimum processing conditions of temperature and strain rate are those corresponding to the maximum or peak in J. The instability criterion developed by Prasad is based on the irreversible thermodynamics of large plastic flow proposed by Ziegler (1963). In terms of the maximum rate of entropy production in material system, the instability criterion is derived by $\xi(\dot{\varepsilon}) = \frac{\partial \ln m/(1+m)}{\partial \ln \dot{\varepsilon}} + m < 0$. Although the processing maps based on DMM have been widely used to optimize the processing parameters in hot forming of metallic materials, the physical interpretation of the dissipator content G and the dissipator co-content J have been re-examined by Montheillet, Jonas and Neale (1996) and Ghosh (2000, 2002). Narayana Murty and co-workers pointed out that the strain rate sensitivity exponent m may vary as a function of strain rate and deformation temperature in complicated alloy systems. As a result, the flow stress does not obey power law ($\sigma = K\dot{\varepsilon}^m$). Therefore, the calculation of efficiency of power dissipation η was extended using the follow expression $\eta = 2(1 - \frac{1}{\sigma\dot{\varepsilon}} \int_0^{\dot{\varepsilon}} \sigma d\dot{\varepsilon})$ and a simple instability condition ($0 < \eta < 2m$) was applied to delineate the unstable regions in a variety of materials based on the modified dynamic materials modeling [Narayana Murty and Nageswara Rao (1998a, 1998b, 1999, 2000, 2002); Narayana Murty, Nageswara Rao and Kashyap (2000, 2002, 2003, 2004, 2005a, 2005b)]. As already mentioned, the constitutive model ($\sigma = K\dot{\varepsilon}^m$) does not always represent accurately the flow stress, and can not reflect the effect of microstructure evolution on the flow stress in hot forming processes. However, a number of studies indicated that the microstructure in hot forming processes is sensitive to the processing parameters [Bakkaloğlu (2002); Bak-Misiuk, Misiuk, Romanowski, Barcz, Jakiela, Dynowska, Domagala and Caliebe (2009); Chen, Hao and Li (2007); Ding, Guo and Wilson (2002); Garbacz, Mizera and Wyrzykowski (1997); Geetha, Singh, Muraleedharan, Gogia and Asokamani (2001); Ma, Lu, Qin and Zhang (2006); Zeng, Shu, Zhang, Zhou, Zhao, Wu, Dai, Yang and Zhou (2008); Zrník, Kvackaj, Pongpaybul, Sricharoenchai, Vilk and Vrchovinsky (2001)]. Also, Sagar (2006) has recently shown that the microstructure of Ti_3Al base aluminide alloys has a significant effect on the unstable regions. And, Luo, Li, Yu and Li (2009) found that the strain affects the processing maps and the unstable regions due to the microstructure evolution at different strains. Therefore, it is concluded that the processing maps proposed by Prasad do not more precisely represent the hot workability in hot forming processes for the absence of considering the microstructure evolution. The purpose of this work is to develop the microstructure-based viscoplastic constitutive equations with the help of internal state variables. Applying the constitutive equations to the calculation of the efficiency of power dissipation and instability criterion, the processing maps taking into account the contribution of strain and microstructure evolution are finally established so as to provide more appropriately physical interpretation and optimize

the processing conditions.

In the present study, a set of microstructure-based viscoplastic constitutive equations are firstly established, in which the dislocation density and grain size of matrix phase are taken as internal state variables. The material constants in constitutive equations are identified by a genetic algorithm (GA)-based objective optimization technique. The efficiency of power dissipation is calculated on the basis of dynamic materials modeling (DMM) and the present constitutive equations. A novel instability criterion considering the grain size and dislocation density is proposed to delineate the regions of flow instabilities with the help of the law of classical thermodynamic and Ziegler's continuum principles. Applying the efficiency of power dissipation and instability criterion to the isothermal compression of Ti-6Al-4V alloy, the processing maps of Ti-6Al-4V alloy at different strains are acquired and the optimum processing conditions are suggested.

2 The efficiency of power dissipation

According to the DMM, the power per unit volume P absorbed by the workpiece material during plastic flow is described as follows:

$$P = G + J = \sigma\dot{\varepsilon} \tag{1}$$

where G represents the power dissipated by plastic work, most of which is converted into viscoplastic heat, the little remaining power being stored as lattice defects[Narayana Murty and Nageswara Rao (1998c)]. The dissipator content G is expressed as:

$$G = \int_0^{\dot{\varepsilon}} \sigma d\dot{\varepsilon} \tag{2}$$

The dissipator co-content J related to the microstructure evolution is given by:

$$J = \int_0^{\sigma} \dot{\varepsilon} d\sigma \tag{3}$$

For an ideal linear dissipator, the maximum dissipator co-content is written as:

$$J_{\max} = \frac{P}{2} = \frac{\sigma\dot{\varepsilon}}{2} \tag{4}$$

The efficiency of power dissipation is defined as:

$$\eta = \frac{P-G}{J_{\max}} = \frac{2(\sigma\dot{\varepsilon} - \int_0^{\dot{\varepsilon}} \sigma d\dot{\varepsilon})}{\sigma\dot{\varepsilon}} \tag{5}$$

where η is a dimensionless parameter, σ is the flow stress (MPa), $\dot{\varepsilon}$ is the strain rate (s^{-1}). The variation of dimensionless parameter η with deformation temperature, strain rate and strain constitutes an iso-efficiency contour map.

Over the years, many types of constitutive equations have been developed to model the deformation behavior of metals and alloys. However, the average grain size d in many of these equations is not considered. It is well known that the microstructure of alloys undergoes a series of dynamic changes in hot forming processes and the evolving microstructure in its turn affects the deformation. In order to more precisely describe the deformation behavior of materials, in this study we establish a set of microstructure-based constitutive equations that consider the dislocation density and the grain size. The constitutive equations are more suitable for the forging processes of metals or alloys in which texture evolution can be ignored for large deformations. And, the flow stress is described following [Chaboche and Jung (1997); Chaboche and Nouailhas (1989); Cheong, Lin and Ball (2001); Dunne (1998); Lin and Dunne (2001); Lin and Yang (1999)]. The physically-based viscoplastic constitutive equations coupling the grain size and the dislocation density are given by the following expression:

$$\begin{aligned}
&\dot{\rho} = \alpha_1 \sqrt{\rho}\,|\dot{\varepsilon}_p| - \alpha_2 e^{-\frac{Q_{dm}}{RT}} \rho \\
&\dot{d} = \beta_0 d^{-\gamma_0} T^{-1} e^{-\frac{Q_{pd}}{RT}} + \beta_1 |\dot{\varepsilon}_p| d^{-\gamma_1} - \beta_2 \dot{\rho}^{\gamma_3} d^{\gamma_2} \\
&\dot{\varepsilon}_p = A \exp(-\frac{Q}{RT}) \left[\frac{\sigma - r - k_0}{K}\right]^n d^{-u} \\
&r = q[\exp(-b\varepsilon_p) + 1] \\
&\sigma = E(\varepsilon_T - \varepsilon_p)
\end{aligned} \tag{6}$$

where ρ is the dislocation density (mm^{-2}), d is the average grain size (μm), the average grain size d and the dislocation density ρ in present equations are treated as internal state variables, r is an internal variable to describe the isotropic hardening/softening behavior (MPa), ε_T is the true total strain, ε_p is the true plastic strain, $\dot{\varepsilon}_p$ is the plastic strain rate, T is the absolute deformation temperature in Kelvin (K), R is the gas constant (8.314 J/(mol·K)), Q_{dm} is the activation energy for cross-slip and recombination (kJ/mol), Q_{pd} is the boundary diffusion activation energy (kJ/mol), Q is the apparent activation energy for deformation (kJ/mol), α_1, α_2, β_0, β_1, β_2, γ_0, γ_1, γ_2, γ_3, A, u, K, q and b are the material constants, k_0 denotes the initial yield stress (MPa), and n is inversely identical to the strain rate sensitivity exponent m ($n = 1/m$), The Young's modulus E (MPa) is given by:

$$E = 2\mu(T)(1+\upsilon) \tag{7}$$

where υ is the Poisson's ratio which is effectively 0.5 in viscoplastic deformation processes, and $\mu(T)$ is the temperature-dependent shear modulus (MPa) expressed as [Varshni (1970)]:

$$\mu(T) = \mu_0 - \frac{e}{\exp(T_r/T) - 1} \tag{8}$$

where μ_0, e and T_r are the material constants.

For isothermal processes, equation (6) simplifies as:

$$\dot{\rho} = \alpha_1 \sqrt{\rho}\,|\dot{\varepsilon}_p| - \alpha_2 \rho$$
$$\dot{d} = \beta_0 d^{-\gamma_0} + \beta_1 |\dot{\varepsilon}_p| d^{-\gamma_1} - \beta_2 \dot{\rho}^{\gamma_3} d^{\gamma_2}$$

$$\dot{\varepsilon}_p = A \left[\frac{\sigma - r - k_0}{K} \right]^n d^{-u} \tag{9}$$

$$r = q[\exp(-b\varepsilon_p) + 1]$$

$$\sigma = E(\varepsilon_T - \varepsilon_p)$$

Substituting Eq. (9) into Eq. (5), the efficiency of power dissipation η for isothermal processes is obtained as:

$$\eta = \frac{P - G}{J_{\max}} = \frac{2(\sigma\dot{\varepsilon} - \int_0^{\dot{\varepsilon}} \sigma d\dot{\varepsilon})}{\sigma\dot{\varepsilon}} = 2 - \frac{2\int_0^{\dot{\varepsilon}} \left[K(\frac{\dot{\varepsilon}_p d^u}{A})^m + r + k_0 \right] d\dot{\varepsilon}_p}{\sigma\dot{\varepsilon}} \tag{10}$$

where the strain rate sensitivity exponent m is obtained using a cubic spline fit between $\log\sigma$ and $\log\dot{\varepsilon}$. In Section 4, we fit σ, r, k_0, d, K, A and $\dot{\varepsilon}_p$ in Eq. (9) with experiment results. When we use the present theory to calculate the flow stress, the total strain is divided into a number of small strains. The plastic strain ε_p is continuously superimposed and the flow stress at each strain can be given through the integration with smaller integration step. By varying the experiment isothermal temperature, the efficiency of power dissipation η as a function of deformation temperature, strain rate and strain can be obtained and plotted into the iso-efficiency contour map. Based on the analysis of Eq. (9) and Eq. (10), it is also seen that the efficiency of power dissipation η can be predicted by using the present viscoplastic constitutive equations.

3 An instability criterion based on the Ziegler's continuum principles

Before introducing the instability criterion based on the Ziegler's continuum principles, we set out related fundamental laws of thermodynamics as:

(I) For a mechanical and conservative system in which the kinetic energy of the molecules is zero, the First Law of Thermodynamics (the balance of energy) is expressed as [Ziegler (1963)]:

$$dW = dU = \sigma_{ij} d\varepsilon_{ij} \tag{11}$$

where W and U are the mechanical work input and the internal energy of the system, respectively. The internal energy depends on strain ε, entropy s and internal state variables related to isotropic hardening/softening behavior [de Sciarra (2008)].

(II) The Second Law of Thermodynamics states that the entropy production s is never negative. i.e.,

$$d^{(i)}s \geq 0 \tag{12}$$

where the equality sign holds for reversible processes and the inequality sign for irreversible ones. The inequality (12) justifies the term 'irreversible processes' involving an entropy production. Alternatively and more often, the second law is put in the form of the Clausius-Duhem inequality as [Voyiadjis and Abu Al-Rub (2003)]:

$$\sigma_{ij}\dot{\varepsilon}_{ij} - \rho_m(\dot{\psi} + s\dot{T}) - q_i \frac{T_{,i}}{T} \geq 0 \tag{13}$$

where σ_{ij} is the Cauchy stress tensor, $\dot{\varepsilon}$ is the total strain rate, ρ_m is the material density, q_i is the heat flux vector, $T_{,i}$ is the temperature gradient, and ψ is the Helmholtz free energy defined as [Thamburaja and Ekambaram (2007); Voyiadjis and Abed (2006); Ziegler (1963)]:

$$\psi = U - sT, \tag{14}$$

or in its rate form [Fagerström and Larsson (2008)]:

$$\dot{\psi} = \dot{U} - \dot{s}T - s\dot{T}. \tag{15}$$

Substituting the time derivative of Eq. (11) into Eq. (15), and assuming no temperature rise in isothermal processes of metals and alloys, i.e., $\dot{T} = 0$, the differentiation of the Helmholtz free energy ψ with respect to time t can further be simplified as:

$$\dot{\psi} = \sigma\dot{\varepsilon} - \dot{s}T \tag{16}$$

Following Rayleigh (1873, 1945), the dissipation function of the system D is defined by Ziegler as (1963):

$$D = T\frac{d^{(i)}S}{dt} \geq 0 \tag{17}$$

Upon substituting Eq. (16) into Eq. (17), D reduces to [Polizzotto (2008); Rajagopal and Srinivasa (1998)]:

$$D = \sigma\dot{\varepsilon}_p - \dot{\psi}_p = T\frac{d^{(i)}S}{dt} \geq 0 \tag{18}$$

Hence, the difference between the mechanical power and the increasing rate of the Helmholtz free energy defines the rate of plastic dissipation.

The Helmholtz free energy can be interpreted as the thermodynamic state potential associated with current state of the material and the deformation gradient referring to the natural configuration. The choice of the form of Helmholtz free energy function ψ is very important since it constitutes the basis in deriving the constitutive equations [Voyiadjis and Deliktas (2009)]. Over the past several decades, many studies have been carried out to model the Helmholtz free energy, and its functional form is usually defined as a quadratic form of its internal state variables [Abu Al-Rub (2008); Bellenger and Bussy (2001); Harrysson, Harrysson and Ristinmaa (2007); Hayakawa, Murakami and Liu (1998); Houlsby and Puzrin (2000); Lubarda (2004); Mahnken, Shaban, Potente and Wilke (2008); Shaban, Mahnken, Wilke, Potente and Ridder (2007)].

In the present study, only the plastic part of Helmholtz free energy is considered. Moreover, the partial differentiation of plastic Helmholtz free energy ψ_p with respect to the viscoplastic internal state variable p is defined as:

$$r = \frac{\partial\psi_p}{\partial p} \tag{19}$$

where r is an internal variable to describe the isotropic hardening/softening behavior (MPa), and it can be described by the following assumed exponent form:

$$r = q[\exp(-b\varepsilon_p) + 1] \tag{20}$$

to capture the isotropic softening effect.

The time derivative of Eq. (19) is given by

$$\dot{\psi}_p = r\dot{p} \tag{21}$$

where $\dot{p} = \sqrt{\frac{2}{3}\dot{\varepsilon}_{ij}^{p}\dot{\varepsilon}_{ij}^{p}}$ is the effective plastic strain rate. For uniaxial tension or compression loading and more generally, in proportional loading, if the plastic strain increment in the direction of loading is $\dot{\varepsilon}_p$ and since the plastic strain is assumed to be incompressible, the effective plastic strain rate $\dot{p}$ becomes to the following form:

$$\dot{p} = \sqrt{\frac{2}{3}\dot{\varepsilon}_{ij}^{p}\dot{\varepsilon}_{ij}^{p}} = \dot{\varepsilon}_p \tag{22}$$

Taking Eq. (22) and Eq. (21) into Eq. (18), the plastic dissipation function of the system is finally expressed as:

$$D = (\sigma - r)\dot{\varepsilon}_p \tag{23}$$

where the plastic strain rate $\dot{\varepsilon}_p$ is obtained by Eq. (9), i.e. $\dot{\varepsilon}_p = A\left[\frac{\sigma - r - k_0}{K}\right]^n d^{-u}$.

In the present study, the instability criterion is developed based on some extremum principles in irreversible thermodynamics with application to continuum mechanics in large plastic flow developed by Ziegler. Ziegler observed that a system undergoing large plastic deformation would be unstable if the differential quotient $dD/d\dot{\varepsilon}$ satisfies the inequality:

$$\frac{dD}{d\dot{\varepsilon}} < \frac{D}{\dot{\varepsilon}} \tag{24}$$

Eq. (24) can be written in the following form:

$$\xi = \frac{\partial \ln D}{\partial \ln \dot{\varepsilon}} - 1 < 0 \tag{25}$$

where ξ is an instability parameter.

By using Eq. (23) and Eq. (25), the instability parameter is expressed as:

$$\xi = \frac{\partial \ln D}{\partial \ln \dot{\varepsilon}} - 1 = \frac{\partial \ln(Ad^{-u}(\sigma - r)[\frac{\sigma - r - k_0}{K}]^n)}{\partial \ln \dot{\varepsilon}} - 1 < 0 \tag{26}$$

The instability parameter is obtained using Eq. (26) at different deformation temperatures, strain rates and strains based on the experimental results. Then the flow instability map is developed to delineate the unstable regions in hot forming processes of material. According to above-presented equations, it can be seen that the present instability criterion ($\xi = \frac{\partial \ln D}{\partial \ln \dot{\varepsilon}} - 1$<0) takes into account the contribution of strain and microstructure.

Finally the processing maps at different strains consist of a superimposition of iso-efficiency contour map and flow instability map, in which the iso-efficiency contour map and flow instability map are both developed in a frame of deformation temperature and strain rate.

Table 1: Chemical composition of the as received Ti-6Al-4V alloy (mass fraction in %)

Al	V	Fe	C	N	O	H	Ti
6.50	4.25	0.04	0.02	0.015	0.16	0.0018	Bal.

4 Application to the isothermal compression of Ti-6Al-4V alloy

4.1 Experiments and results

The chemical composition and micrograph of as received Ti-6Al-4V alloy are shown in Table 1 and Fig.1 respectively. The starting microstructure consists of an equiaxed primary α phase (hexagonal close-packed, hcp) with about a grain size of 10.0 μm, secondary (platelet) α and a small amount of intergranular β (body-centered cubic, bcc). The heat treatment prior to isothermal compression was conducted in the following procedures: (1) heating to 1023 K and holding for 1.5 h, (2) air-cooling to room temperature. The cylindrical compression specimens have 8.0 mm in diameter and 12.0 mm in height, and the cylinder ends were grooved for retention of glass lubricants in isothermal compression of Ti-6Al-4V alloy. The beta-transus temperature for this alloy was determined to be 1263 K [Luo, Li, Li and Yu (2009)], which is in a good agreement with that reported in the reference [Semiatin and Bieler (2001)].

To investigate the effect of processing parameters on the deformation behavior of Ti-6Al-4V alloy, isothermal compressions were conducted on a Thermecmaster-Z simulator in the deformation temperature ranging from 1093 K to 1303 K, the strain rates of 0.001, 0.01, 0.1, 1.0, and 10.0 s^{-1}, and the height reduction ranging from 20% to 60% with an interval of 10%. The specimens prior to isothermal compression were heated and held for 3.0 min at the deformation temperature so as to obtain a uniform deformation temperature. The stress-strain curves were recorded automatically in isothermal compression. After isothermal compression, the specimens were cooled in air to room temperature.

In order to measure the grain size of isothermally compressed Ti-6Al-4V alloy, the isothermally compressed specimens were axially sectioned and prepared using standard metallographic techniques. Four measurement points and four visual fields of one point in the different deformation regions were chosen. The grain size was measured at an OLYMPUS PMG3 microscope with the quantitative metallography SISC IAS V8.0 image analysis software, and the primary α grain size was calculated by the average value of sixteen visual fields.

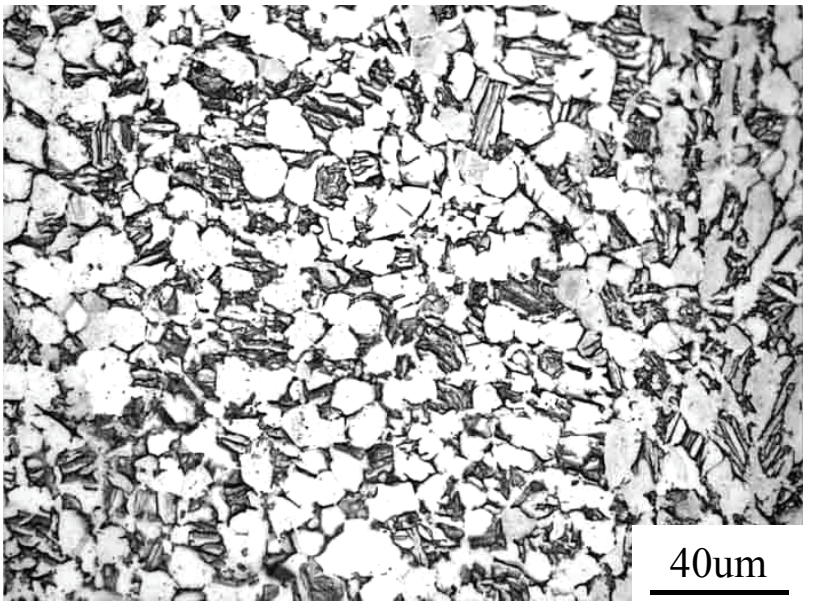

Figure 1: Micrograph of the as received Ti-6Al-4V alloy

4.1.1 Flow stress

Selected flow stress curves in the α+β two-phase region and β single-phase region of Ti-6Al-4V alloy at different strain rates and deformation temperatures are shown in Fig. 2. From Fig. 2, it can be seen that in the α+β two-phase region (<1263 K) at higher strain rates (>0.1 s^{-1}) the flow stress increases quickly with the strain and reaches a peak. It then decreases to a steady value as the dynamic softening is sufficient to counteract the hardening of the material in the compression process. On the other hand, in the α+β two-phase region (<1263 K) at lower strain rates ($\leq$0.01 s^{-1}) and in the β single-phase region (>1263 K) at any given strain rates the curves are of steady-state type, which indicates that the mechanisms of softening are sufficiently fast to balance the rate of work hardening. In addition, it is also observed that the flow stress decreases with the increasing of the deformation temperature at the certain strain rate, and increases with the increasing of the strain rate at the certain temperature. In other words, the flow stress is sensitive to strain rate and deformation temperature in isothermal compression of Ti-6Al-4V alloy.

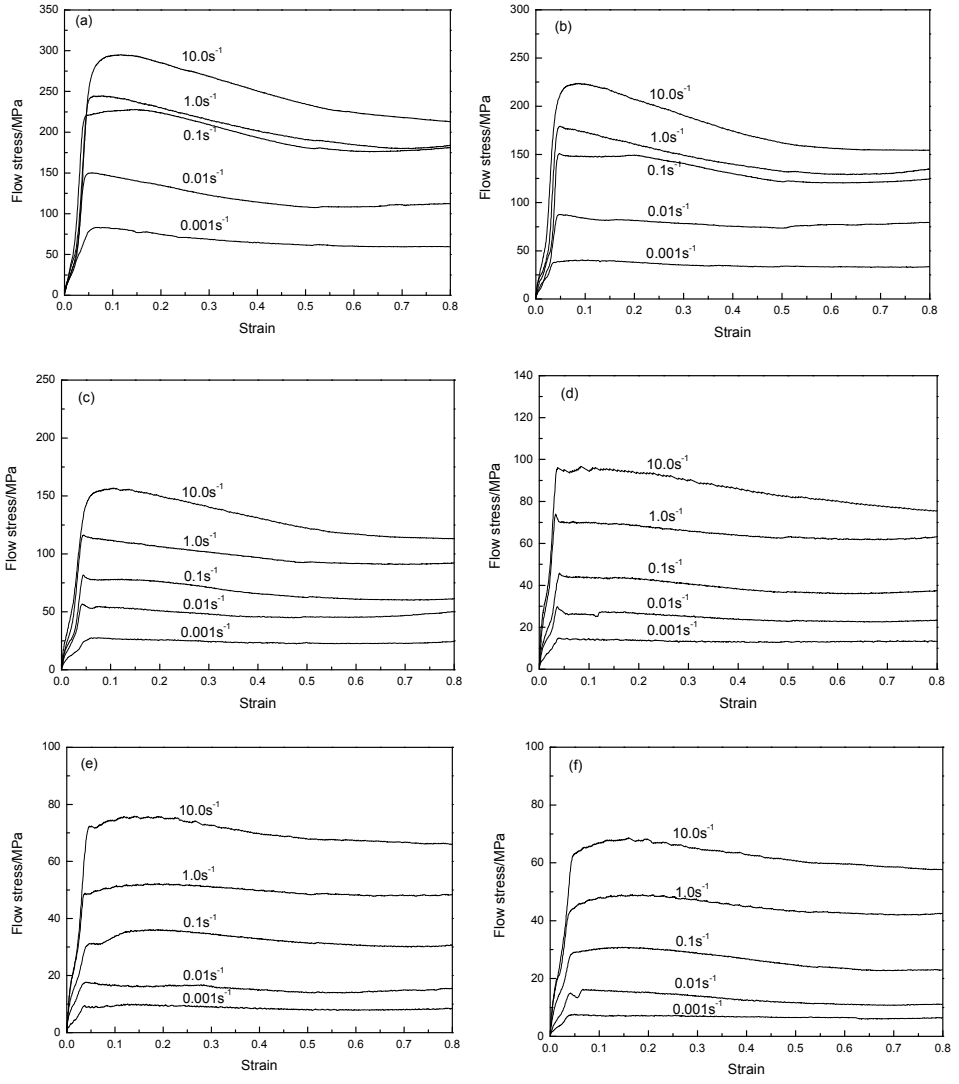

Figure 2: Selected stress-strain curves in isothermal compression of Ti-6Al-4V alloy at the deformation temperatures of 1093 K (a), 1143 K (b), 1183 K (c), 1223 K (d), 1263 K (e), and 1303 K (f)

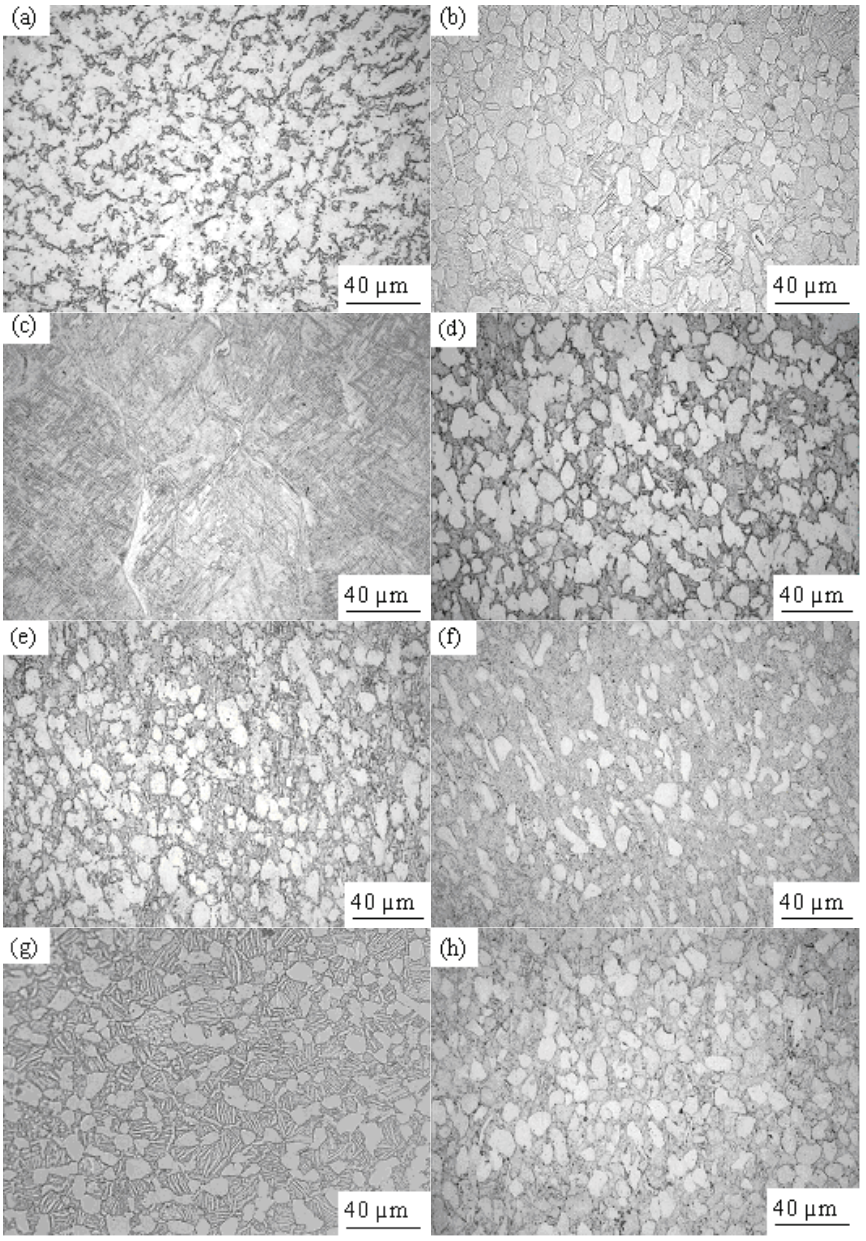

Figure 3: Micrographs of the isothermally compressed Ti-6Al-4V alloy at the different conditions T=1093 K, $\dot{\varepsilon}$=0.001 s^{-1}, ε=50% (a); T=1223 K, $\dot{\varepsilon}$=0.001 s^{-1}, ε=50% (b); T=1293 K, $\dot{\varepsilon}$=0.001 s^{-1}, ε=50% (c); $\dot{\varepsilon}$=0.001 s^{-1}, T=1203 K, ε=60% (d); $\dot{\varepsilon}$=0.01 s^{-1}, T=1203 K, ε=60% (e); $\dot{\varepsilon}$=1.0 s^{-1}, T=1203 K, ε=60% (f); ε=20%, T=1183 K, $\dot{\varepsilon}$=10.0 s^{-1}(g); ε=60%, T=1183 K, $\dot{\varepsilon}$=10.0 s^{-1} (h). The compression axis is horizontal in all the micrographs

4.1.2 Microstructure evolution

The microstructure of Ti-6Al-4V alloy at different deformation temperatures, strain rates and height reductions is shown in Fig. 3. Fig. 3(a)-(c) shows the effect of deformation temperature on the microstructure in isothermal compression of Ti-6Al-4V alloy. As shown in Fig. 3(a)∼(c), the α phase begins to transform into β phase with the increasing of the deformation temperatures ranging from 1093 K to 1223 K, resulting in the decreasing volume fraction of α phase. Meanwhile, the bigger α phase diffuses towards the β phase in high deformation temperature, which leads to the decreasing of grain size of α phase. At a deformation temperature of 1293 K, the α phase has been transformed to the β phase completely and the lamellar structure can be only observed. The effect of strain rate on the microstructure in isothermal compression of Ti-6Al-4V alloy is presented in Fig. 3(d)-(f). It can be seen from Fig. 3(d)-(f) that the microstructure is composed of equiaxed primary α phase and intergranular β at a strain rate of 0.001 s^{-1}. When the strain rate is up to 1.0 s^{-1}, the microstructure has slight oriented characteristic. Moreover, it is also observed that the volume fraction of primary α phase decreases with the increasing of the strain rate. This phenomenon is possibly related to the deformation heat. Fig. 3(g)-(h) shows the effect of height reduction on the microstructure in isothermal compression of Ti-6Al-4V alloy. As illustrated in Fig. 3(g), the microstructure consists of equiaxed primary α phase surrounded by lamellar α structure and a small amount of intergranular β phase at a height reduction of 20%. When the height reduction is up to 60% illustrated in Fig. 3(h), the lamellar α structure disappears essentially and the microstructure consists of equiaxed primary α phase and a small amount of intergranular β phase. As the above-discussed, the processing parameters including the deformation temperature, strain rate and height reduction will significantly affect the microstructure of isothermally compressed Ti-6Al-4V alloy, so the processing maps of Ti-6Al-4V alloy representing 'safe' and 'non-safe' hot working processing conditions should be established to achieve microstructural control.

The grain size of primary α phase of isothermally compressed Ti-6Al-4V alloy at different deformation temperatures, strain rates and height reductions is shown in Table 2. From Table 2, it is seen that the processing parameters have some influence on the grain size of primary α phase.

According to the experimental results, it is observed that the microstructure of Ti-6Al-4V alloy used in present investigation changes dynamically and the microstructure evolution has some effect on the deformation behavior of Ti-6Al-4V alloy in high temperature deformation. So the authors adopt the present power dissipation efficiency equation and instability parameter equation to establish the processing maps of isothermally compressed Ti-6Al-4V alloy so as to obtain the processing

Table 2: The grain size of primary α phase at different deformation temperatures, strain rates and height reductions

Deformation temperature (K)	Strain rate (s^{-1})	Height reduction (%)	Grain size (μm)
1093	1.0	20	12.68
1093	0.001	50	10.90
1123	10.0	30	12.17
1123	0.1	60	11.98
1143	0.01	40	11.20
1143	0.001	50	10.60
1143	0.01	20	10.94
1163	1.0	40	10.03
1163	0.1	30	10.20
1163	0.001	50	11.09
1183	10.0	20	9.74
1183	0.001	60	9.65
1183	0.1	40	10.47
1203	0.01	50	9.52
1203	0.1	30	8.58
1223	1.0	20	7.52
1223	0.1	60	6.91
1233	10.0	30	6.71
1233	0.001	40	8.74

conditions and achieve the microstructural control of Ti-6Al-4V alloy in hot forming.

4.2 Identification of material constants

The material constants in physically-based viscoplastic constitutive equations are identified by using a GA-based objective optimization technique. Using the conventional optimization method, it is very difficult to search for the global minimum in the multi-modal distribution space. The GA method is a stochastic search method based on evolution and genetics, and exploits the concept of the survival of the fittest [DeJong (1999)]. For a given problem, there exists a multitude of possible solutions that form a solution space. In GA, a highly effective search of the solution space is performed, allowing a population of strings representing the possible solutions to evolve through the basic random operators of selection,

Table 3: Domains of the material constants in the constitutive equations of Ti-6Al-4V alloy

$0.1 \leq \alpha_1 \leq 100.0$	$1.0\times10^{-12} \leq \alpha_2 \leq 2.0$	$0.01 \leq \beta_0 \leq 1000.0$	$0.01 \leq \beta_1 \leq 100.0$	$1.0\times10^{-6} \leq \beta_2 \leq 1.0$
$1.0 \leq \gamma_0 \leq 1.0\times10^{8}$	$0.01 \leq \gamma_1 \leq 10.0$	$1.0\times10^{-6} \leq \gamma_2 \leq 10.0$	$0.5 \leq \gamma_3 \leq 10.0$	$1.0 \leq q \leq 50.0$
$0.5 \leq b \leq 10.0$	$1.0\times10^{-6} \leq A \leq 10.0$	$1.0 \leq K \leq 2000.0$	$0.1 \leq k_0 \leq 4.0$	$1.0 \leq u \leq 2.5$

crossover, and mutation [Castro, António and Sousa (2004)]. Therefore, a GA-based optimization technique is used to determine the material constants in present constitutive equations. Optimization technique for obtaining the material constants in physically-based viscoplastic constitutive equations is based on minimizing the sum of the squares of the errors between the experimental and calculated data [Lin, Liu, Farrugia and Zhou (2005)]. For present constitutive equations, two objective functions are defined in terms of the square of the difference between the experimental and the predicted data for grain size of prior α phase and flow stress in the following form:

$$f_1(x) = \sum_{k=1}^{l_1} \sum_{j=1}^{n_1} \sum_{i=1}^{m_1} w_{ijk} \left(\left(\left(d_i^c \right)_j \right)_k - \left(\left(d_i^e \right)_j \right)_k \right)^2 \tag{27}$$

$$f_2(x) = \sum_{h=1}^{l_2} \sum_{q=1}^{n_2} \sum_{p=1}^{m_2} w_{pqh} \left(\left(\left(\sigma_p^c \right)_q \right)_h - \left(\left(\sigma_p^e \right)_q \right)_h \right)^2 \tag{28}$$

where $f_1(x)$ and $f_2(x)$ are the residuals for grain size and flow stress, $x(x = [x_1, x_2, \ldots, x_s])$ represent the material constants, s is the number of the constants to be determined, $\left(\left(d_i^c \right)_j \right)_k$ and $\left(\left(d_i^e \right)_j \right)_k$ are the predicted and experimental grain size at time i, strain rate j and deformation temperature k. The predicted grain size $\left(\left(d_i^c \right)_j \right)_k$ is obtained from the grain growth Eq. (9) by means of a numerical integration method, m_1 is the number of the experimental average grain size at deformation temperature k and strain rate j, n_1 is the number of strain rate, l_1 is the number of deformation temperature, and w_{ijk} is the weight coefficient. Similarly, $\left(\left(\sigma_p^c \right)_q \right)_h$ and $\left(\left(\sigma_p^e \right)_q \right)_h$ are the predicted and experimental flow stress at time p, strain rate q and deformation temperature h. The predicted flow stress $\left(\left(\sigma_p^c \right)_q \right)_h$ is obtained from the flow stress Eq. (9), m_2 is the number of the experimental flow stress at deformation temperature h and strain rate q, n_2 is the number of strain rate, l_2 is the number of deformation temperature, and w_{pqh} is the weight coefficient.

So the material constants in present constitutive equations can be obtained on the basis of the experimental flow stress and grain size in the deformation temperature ranging from 1093 K to 1303 K, the strain rates of 0.001, 0.01, 0.1, 1.0, and 10.0 s^{-1}, and the height reduction ranging from 20% to 60% with an interval 10%. For Ti-6Al-4V alloy used in present investigation, Q_{pd} is 677.37 kJ/mol [Luo, Li, Li and Yu (2009)], Q_{dm} is 20 kJ/mol, μ_0 is 49.02 GPa, e is 5.821 GPa, T_r is 181 K [Picu and Majorell (2002)].

The domains of the material constants are given in this study in order to accelerate the convergence to the global optimum point. And, the domains of the material

constants can be determined from their physical significance. For some constants, it is difficult to determine their variation regions. In this case, a relatively large variation range can be given [Lin and Yang (1999)]. The domains of the material constants in present constitutive equations of Ti-6Al-4V alloy are listed in Table 3.

5 The processing maps of Ti-6Al-4V alloy

After identifying the material constants in present constitutive equations, the efficiency of power dissipation η and the instability parameter ξ can be obtained at different deformation temperatures, strain rates and strains using Eq. (10) and Eq. (26). Then the processing maps of isothermally compressed Ti-6Al-4V alloy at different strains are established and shown in Fig. 4.

Fig. 4(a)-(e) show the processing maps of Ti-6Al-4V alloy constructed in the deformation temperature ranging from 1093 K to 1303 K and strain rate ranging from 0.001 s^{-1} to 10.0 s^{-1} at the strains of 0.3, 0.4, 0.5, 0.6 and 0.7 with microstructural observation. As seen from Fig. 4(a)-(e), the instability domains of Ti-6Al-4V alloy vary with the increasing of strain. When the strain ranges from 0.3 to 0.6, the instability domain of Ti-6Al-4V alloy only occurs at higher deformation temperatures (>1195 K) and higher strain rates (>0.41 s^{-1}). However, this alloy at a strain of 0.7 exhibits three instability domains as follows: the first one is in the deformation temperature ranging from 1297 K to 1303 K and the strain rate ranging from 0.69 s^{-1} to 10.0 s^{-1}, the second one is in the deformation temperature ranging from 1180 K to 1240 K and the strain rate ranging from 0.77 s^{-1} to 10.0 $s^{-1}$and the last one is in the deformation temperature ranging from 1093 K to 1130 K and the strain rate ranging from 0.047 s^{-1} to 10.0 s^{-1}. This phenomenon can be clearly explained based on the analysis of the deformation behavior at higher deformation temperatures and higher strain rates and the microstructure evolution of isothermally compressed Ti-6Al-4V alloy. At higher deformation temperatures, the work hardening only occurs at quite small strain (approximately less than 10%). The softening effect is sufficiently fast to balance the work hardening effect. The flow stress curves represent steady-state type shown in Fig. 2. Moreover, at higher strain rates the deformation heat does not have time to be conducted in tool, resulting in the flow softening becomes dominant in hot forming processes. Thermal softening eliminates the stabilising effect of work hardening and can cause material instability [Bruschi, Poggio, Quadrini and Tata (2004)]. So the instability flow easily occurs at higher deformation temperatures and higher strain rates. Fig. 4(c)1 and 4(e)1 show the microstructure of isothermally compressed Ti-6Al-4V alloy at a deformation temperature of 1203 K and strain rate of 1.0 s^{-1} but with different strain. Fig. 4(c)2 and 4(e)2 show the microstructure of isothermally compressed

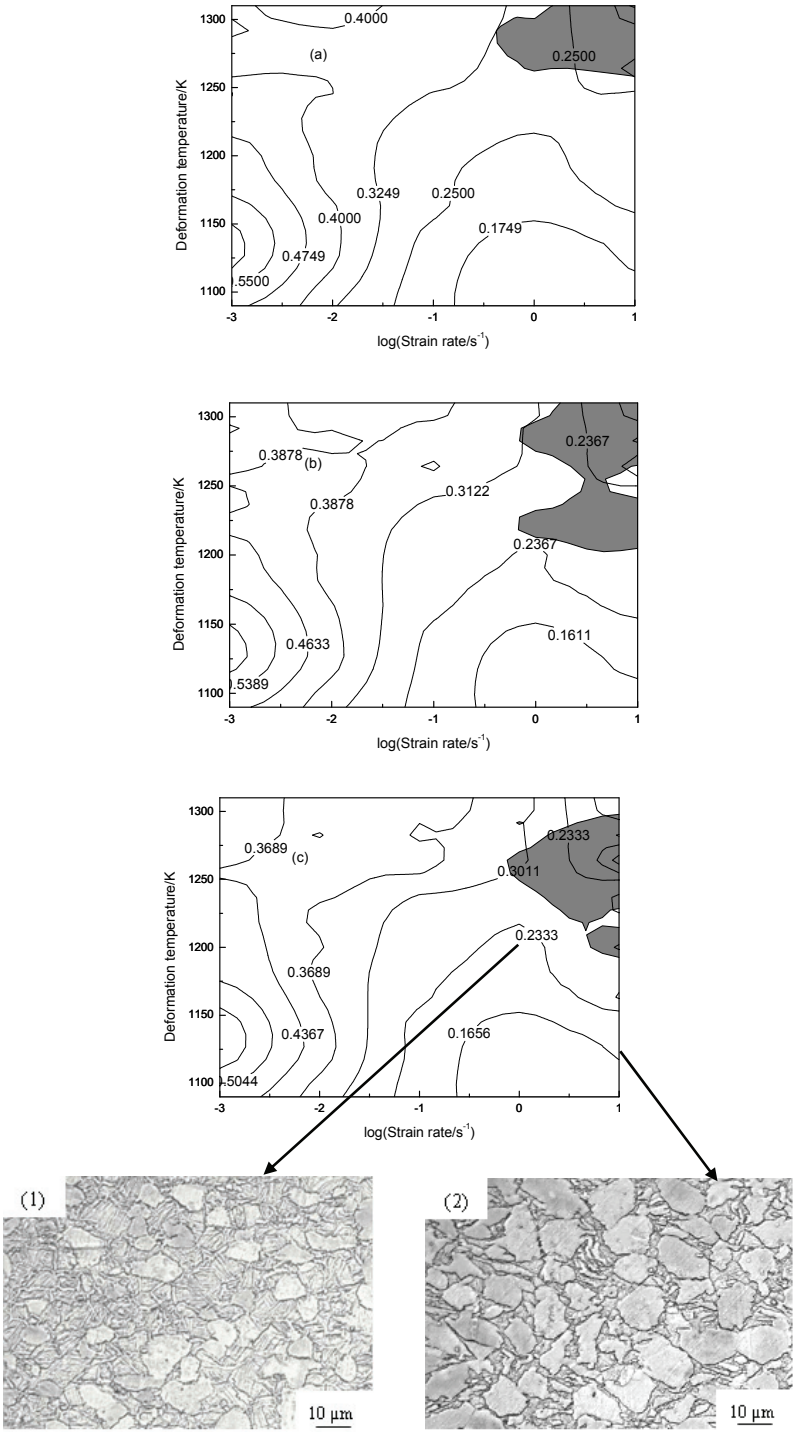
(a)
0.4000
0.2500
0.3249
0.2500
0.4000
0.1749
0.4749
.5500
Deformation temperature/K
log(Strain rate/s^{-1})
(b)
0.2367
0.3878
0.3122
0.3878
0.2367
0.4633
0.1611
.5389
Deformation temperature/K
log(Strain rate/s^{-1})
(c)
0.2333
0.3689
0.3011
0.2333
0.3689
0.4367
0.1656
.5044
Deformation temperature/K
log(Strain rate/s^{-1})
(1)
10 μm
(2)
10 μm

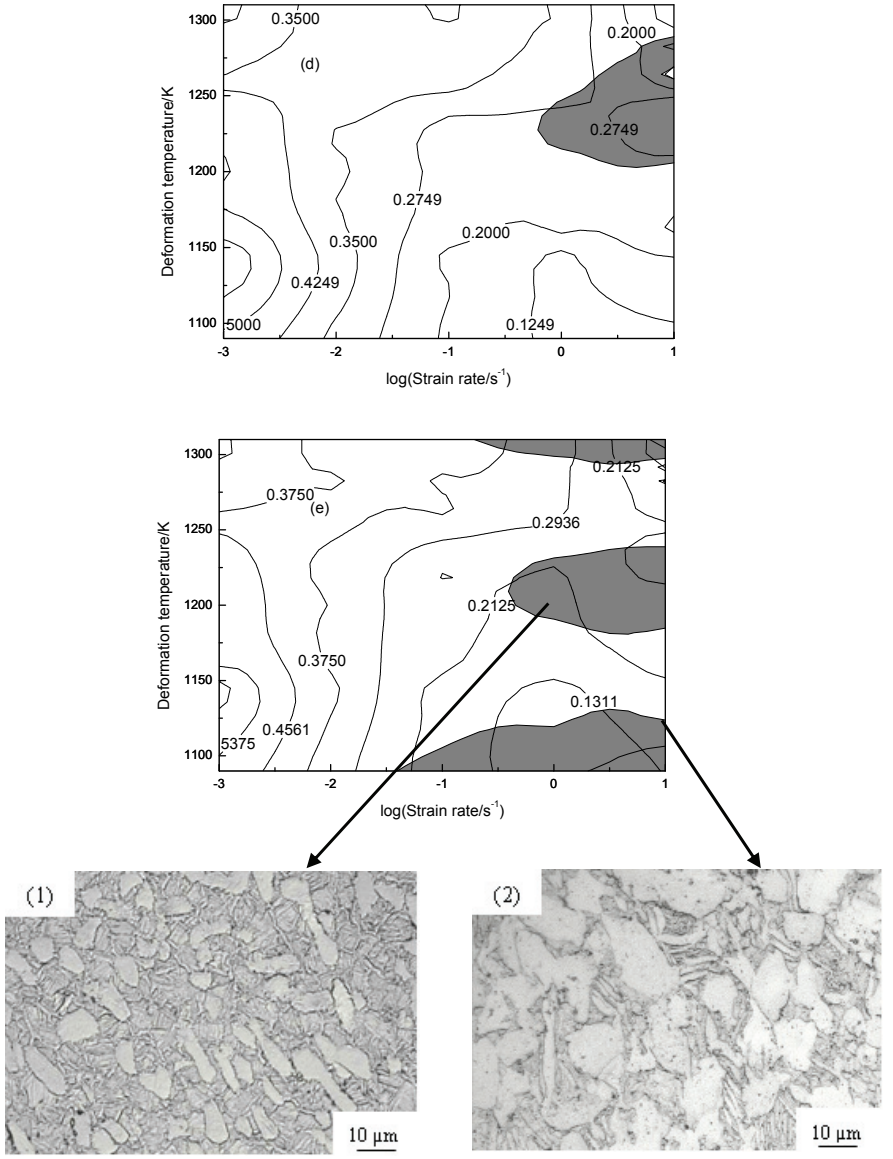

Figure 4: Processing maps and micrographs of the isothermally compressed Ti-6Al-4V alloy at the strains of 0.3 (a), 0.4 (b), 0.5 (c), 0.6 (d), 0.7 (e). Numbers represent efficiency of power dissipation. Shaded areas represent the instability regions

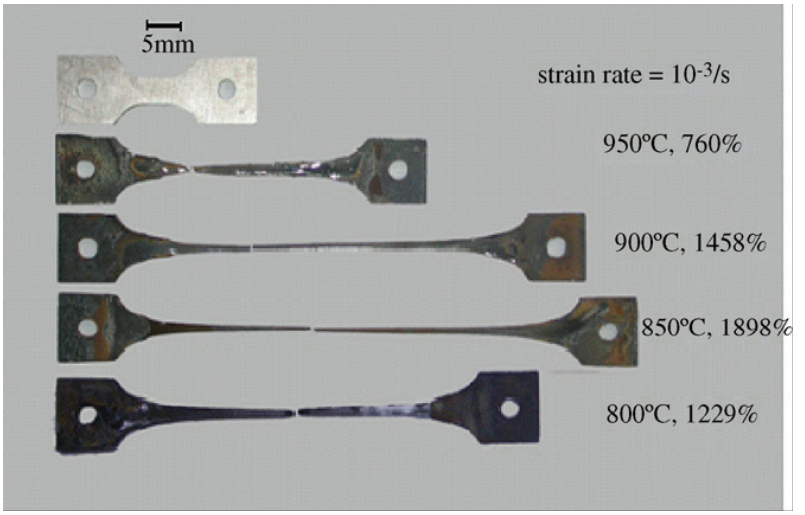

Figure 5: Results of tensile tests at a strain rate of 0.001 s^{-1} [Lee, Yoon, Park, Ko, Shin and Lee (2007)]

Ti-6Al-4V alloy at a deformation temperature of 1123 K and strain rate of 10.0 s^{-1} but with different strain. Compared the micrographs in Fig. 4(c)1 with that in Fig. 4(e)1 and the micrographs in Fig. 4(c)2 with that in Fig. 4(e)2, it is observed that primary α phase of isothermally compressed Ti-6Al-4V alloy is equiaxed at a strain of 0.5. But when the strain is up to 0.7, the microstructure has oriented characteristic. The microstructure of isothermally compressed Ti-6Al-4V alloy undergoes dynamically change as strain increases, which possibly leads to unstable microstructure forms at lower deformation temperatures and higher strain rates. So the processing parameters of Ti-6Al-4V alloy shouldn't be chosen in those instability domains so as to prevent the occurrence of microstructure-based defects.

As seen from Fig. 4(a)-(c), the peak efficiencies of power dissipation at the strains of 0.3, 0.4 and 0.5 are about 0.66, 0.67 and 0.64 respectively, occurring at a deformation temperature of 1123 K and strain rate of 0.001 s^{-1}. But the peak efficiencies of power dissipation at the strains of 0.6 and 0.7 are about 0.67 and 0.68 respectively, occurring at a deformation temperature of 1143 K and strain rate of 0.001 s^{-1}, as illustrated in Fig. 4(d)-(e). The peak efficiencies of power dissipation are correspondent to optimal processing conditions of Ti-6Al-4V alloy. Moreover, the efficiency values as high as 0.60$\sim$0.68 indicate the superplasticity of Ti-6Al-4V alloy. Lee, Yoon, Park, Ko, Shin and Lee (2007) had confirmed that the maximum elongation of 1898% for Ti-6Al-4V alloy was obtained at a deformation tempera-

ture of 1123 K and strain rate of 0.001 s^{-1}, and typical neckfree superplastic elongation of test specimens is shown in Fig. 5. Therefore, the processing parameters in multi-stage forming should be adjusted with the help of the processing maps at different strains so as to realize the precise forming.

On the basis of Prasad's theory, the authors have established the processing maps of Ti-6Al-4V alloy at different strains and reported in the open literature [Luo, Li, Yu and Li (2009)]. Compared the present processing maps with that of reference [Luo, Li, Yu and Li (2009)], it can be observed that the instability domain of present study in the strain ranging from 0.3 to 0.6 only occurs at higher deformation temperatures (>1195 K) and higher strain rates (>0.41 s^{-1}). However, reference indicates that the instability domains not only exhibit at higher deformation temperatures (>1246 K) and higher strain rates (>1.05 s^{-1}), but also at lower deformation temperatures ranging from 1093 K to 1170 K and medium strain rates ranging from 0.011 s^{-1} to 1.72 s^{-1}. The main reason for this difference is that the microstructure in hot forming processes of metals and alloys can be improved and the defects of intrinsic microstructure (grain-boundary cavitation, wedge cracking and cleavage) can disappear under proper processing conditions. And the microstructure has some effect on the flow stress of material. Therefore, the instability parameter using Eq. 26 which considers the contribution of microstructure evolution is different from that based on the Prasad's theory.

6 Conclusions

A set of microstructure-based viscoplastic constitutive equations are proposed with the help of the dislocation density rate equation and the grain growth rate equation. The material constants in viscoplastic constitutive equations are identified by a genetic algorithm (GA)-based objective optimization technique. And the convergence to the global optimum point is faster when the domains of the material constants are given in advance.

The efficiency of power dissipation is developed on the basis of viscoplastic constitutive equations and dynamic materials modelling. The efficiency values are calculated as a function of deformation temperature, strain rate and strain. And, those values can be predicted by using the present viscoplastic constitutive equations.

The instability criterion based on some extremum principles in irreversible thermodynamics takes into account the contribution of strain and microstructure evolution in hot forming processes.

According to the analysis of deformation behavior and microstructure evolution in isothermal compression of Ti-6Al-4V alloy, it is concluded that the effect of strain on the deformation behavior and the microstructure is significant besides the effect

of deformation temperature and strain rate, so the processing maps representing 'safe' and 'non-safe' hot working processing conditions need to be established. Moreover, the effect of strain and microstructure on the processing maps should be considered.

The instability domain of Ti-6Al-4V alloy in the strain ranging from 0.3 to 0.6 only occurs at higher deformation temperatures and higher strain rates. However, this alloy at a strain of 0.7 exhibits three instability domains. The instability domains in instability maps vary with the increasing of strain. Those phenomena are attributed to the changes of deformation behavior and microstructure.

The peak efficiencies of power dissipation at the strains of 0.3, 0.4 and 0.5 occur at a deformation temperature of 1123 K and strain rate of 0.001 s^{-1}. But at the strains of 0.6 and 0.7, those occur at a deformation temperature of 1143 K and strain rate of 0.001 s^{-1}. The peak efficiencies of power dissipation are correspondent to optimal processing conditions of Ti-6Al-4V alloy.

Acknowledgement: The authors thank the financial supports from the National Natural Science Foundation of China with Grant No. 50975234 and the fund of the State Key Laboratory of Solidification Processing in NWPU with Grant No. KP200905.

References

Abu Al-Rub, R. K. (2008): Interfacial gradient plasticity governs scale-dependent yield strength and strain hardening rates in micro/nano structured metals. *Int. J. Plasticity*, vol. 24, no. 8, pp. 1277-1306.

Alexander, J. M. (1989): *Modeling of Hot Deformation of Steel*, Springer-Verlag, Berlin.

Bakkaloğlu, A. (2002): Effect of processing parameters on the microstructure and properties of an Nb microalloyed steel. *Mater. Lett.*, vol. 56, no. 3, pp. 200-209.

Bak-Misiuk, J.; Misiuk, A.; Romanowski; Barcz, A.; Jakiela, R.; Dynowska, E.; Domagala, J. Z.; Caliebe, W. (2009): Effect of processing on microstructure of Si: Mn. *Mater. Sci. Eng. B*, vol. 159-160, pp. 99-102.

Bellenger, E.; Bussy, P. (2001): Phenomenological modeling and numerical simulation of different modes of creep damage evolution. *Int. J. Solids Struct.*, vol. 38, no. 4, pp. 577-604.

Bruschi, S.; Poggio, S.; Quadrini, F.; Tata, M. E. (2004): Workability of Ti-6Al-4V alloy at high temperatures and strain rates. *Mater. Lett.*, vol. 58, no. 27-28, pp. 3622-3629.

Castro, C. F.; António, C. A. C.; Sousa, L. C. (2004): Optimisation of shape and process parameters in metal forging using genetic algorithms. *J. Mater. Process. Technol.*, vol. 146, no. 3, pp. 356-364.

Chaboche, J. L.; Jung, O. (1997): Application of a kinematic hardening viscoplasticity model with thresholds to the residual stress relaxation. *Int. J. Plasticity*, vol. 13, no. 10, pp. 785-807.

Chaboche, J. L.; Nouailhas, D. (1989): A unified constitutive model for cyclic viscoplasticity and its applications to various stainless steel. *J. Engng Mater. Technol. ASME*, vol. 111, pp. 424-430.

Cheong, B. H.; Lin, J.; Ball, A. A. (2001): Modelling of hardening due to grain growth for a superplastic alloy. *J. Mater. Process. Technol.*, vol. 119, no. 1-3, pp. 361-365.

Chen, T. J.; Hao, Y.; Li, Y. D. (2007): Effects of processing parameters on microstructure of thixoformed ZA27 alloy. *Mater. Design*, vol. 28, no. 4, pp. 1279-1287.

DeJong, K. (1999): Evolution computation: recent developments and open issues. In: *Proceedings of the Evolutionary Algorithms in Engineering Computer Science*, Finland, Wiley, Chichester, pp. 43.

de Sciarra, F. M. (2008): A general theory for nonlocal softening plasticity of integral-type. *Int. J. Plasticity*, vol. 24, no. 8, pp. 1411-1439.

Ding, R.; Guo, Z. X.; Wilson, A. (2002): Microstructural evolution of a Ti-6Al-4V alloy during thermomechanical processing. *Mater. Sci. Eng. A*, vol. 327, no. 2, pp. 233-245.

Dunne, F. P. E. (1998): Inhomogeneity of microstructure in superplasticity and its effect on ductility. *Int. J. Plasticity*, vol. 14, no. 4-5, pp. 413-433.

Fagerström, M.; Larsson, R. (2008): A thermo-mechanical cohesive zone formulation for ductile fracture. *J. Mech. Phys. Solids*, vol. 56, no. 10, pp. 3037-3058.

Frost, H. J.; Ashby, M. F. (1982): *Deformation Mechanism Maps: the Plasticity and Creep of Metals and Ceramics*, Pergamon Press, London.

Garbacz, H.; Mizera, J.; Wyrzykowski J. W. (1997): Influence of deformation parameters on microstructures of TiAl alloys. *J. Mater. Process. Technol.*, vol. 64, no. 1-3, pp. 127-132.

Geetha, M.; Singh, A. K.; Muraleedharan, K.; Gogia, A. K.; Asokamani, R. (2001): Effect of thermomechanical processing on microstructure of a Ti-13Nb-13Zr alloy. *J. Alloy. Compd.*, vol. 329, no. 1-2, pp. 264-271.

Gegel, H. L.; Malas, J. C.; Doraivelu, S. M.; Shende, V. A. (1988): *Metals Handbook, Forming and Forging*, vol. 14. ASM International, Ohio.

Ghosh, S. (2000): Interpretation of microstructural evolution using dynamic materials modeling. *Metall. Mater. Trans. A*, vol. 31, no. 11, pp. 2973-2974.

Ghosh, S. (2002): Interpretation of flow instability using dynamic material modeling. *Metall. Mater. Trans. A*, vol. 33, no. 5, pp. 1569-1572.

Harrysson, M.; Harrysson, A.; Ristinmaa, M. (2007): Spatial representation of evolving anisotropy at large strains. *Int. J. Solids Struct.*, vol. 44, no. 10, pp. 3514-3532.

Hayakawa, K.; Murakami, S.; Liu, Y. (1998): An irreversible thermodynamic theory for elastic-plastic-damage materials. *Eur. J. Mech. A/Solids*, vol. 17, no. 1, pp. 13-32.

Houlsby, G. T.; Puzrin, A. M. (2000): A thermomechanical framework for constitutive models for rate-independent dissipative materials. *Int. J. Plasticity*, vol. 16, no. 9, pp. 1017-1047.

Lee, H. S.; Yoon, J. H.; Park, C. H.; Ko, Y. G.; Shin, D. H.; Lee, C. S. (2007): A study on diffusion bonding of superplastic Ti-6Al-4V ELI grade. *J. Mater. Process. Technol.*, vol. 187-188, pp. 526-529.

Lin, J.; Dunne, F. P. E. (2001): Modelling grain growth evolution and necking in superplastic blow-forming. *Int. J. Mech. Sci.*, vol. 43, no. 3, pp. 595-609.

Lin, J.; Liu, Y.; Farrugia, D. C. J.; Zhou, M. (2005): Development of dislocation-based unified material model for simulating microstructure evolution in multipass hot rolling. *Philos. Mag.*, vol. 85, no. 18, pp. 1967-1987.

Lin, J.; Yang, J. B. (1999): GA-based multiple objective optimisation for determining viscoplastic constitutive equations for superplastic alloys. *Int. J. Plasticity*, vol. 15, no. 11, pp. 1181-1196.

Lubarda, V. A. (2004): On thermodynamic potentials in linear thermoelasticity. *Int. J. Solids Struct.*, vol. 41, no. 26, pp. 7377-7398.

Luo, J.; Li, M. Q.; Li, H.; Yu, W. X. (2009): Effect of the strain on the deformation behavior of isothermally compressed Ti-6Al-4V alloy. *Mater. Sci. Eng. A*, vol. 505, no, 1-2, pp. 88-95.

Luo, J.; Li, M. Q.; Yu, W. X.; Li, H. (2009): Effect of the strain on processing maps of titanium alloys in isothermal compression. *Mater. Sci. Eng. A*, vol. 504, no. 1-2, pp. 90-98.

Ma, F. C.; Lu, W. J.; Qin, J. N.; Zhang, D. (2006): Microstructure evolution of near-α titanium alloys during thermomechanical processing. *Mater. Sci. Eng. A*, vol. 416, no. 1-2, pp. 59-65.

Mahnken, R.; Shaban, A.; Potente, H.; Wilke, L. (2008): Thermoviscoplastic modelling of asymmetric effects for polymers at large strains. *Int. J. Solids Struct.*,

vol. 45, no. 17, pp. 4615-4628.

Montheillet, F.; Jonas, J. J.; Neale, K. W. (1996): Modeling of dynamic material behavior: a critical evaluation of the dissipater power co-content approach. *Metall. Mater. Trans. A*, vol. 27, no. 1, pp. 232-235.

Narayana Murty, S. V. S.; Nageswara Rao, B. (1998a): Hot working characteristics of Zr-2·5Nb using processing maps. *Mater. Sci. Technol.*, vol. 14, no. 8, pp. 835-837.

Narayana Murty, S. V. S.; Nageswara Rao, B. (1998b): On the development of instability criteria during hotworking with reference to IN 718. *Mater. Sci. Eng. A*, vol. 254, no. 1-2, pp. 76-82.

Narayana Murty, S. V. S.; Nageswara Rao, B. (1998c): Ziegler's criterion on the instability regions in processing maps. *J. Mater. Sci. Lett.*, vol. 17, no. 14, pp. 1203-1205.

Narayana Murty, S. V. S.; Nageswara Rao, B. (1999): On the flow localization concepts in the processing maps of IN718. *Mater. Sci. Eng. A*, vol. 267, no. 1, pp. 159-161.

Narayana Murty, S. V. S.; Nageswara Rao, B. (2000): On the flow localization concepts in the processing maps of titanium alloy Ti-24Al-20Nb. *J. Mater. Process. Technol.*, vol. 104, no. 1-2, pp. 103-109.

Narayana Murty, S. V. S.; Nageswara Rao, B. (2002): Reinvestigation of dynamic materials model analysis of 99.94% purity aluminium. *Mater. Sci. Technol.*, vol. 18, no. 5, pp. 571-574.

Narayana Murty, S. V. S.; Nageswara Rao, B.; Kashyap, B. P. (2000): Instability criteria for hot deformation of materials. *Int. Mater. Rev.*, vol. 45, no. 1, pp. 15-26.

Narayana Murty, S. V. S.; Nageswara Rao, B.; Kashyap, B. P. (2002): Processing maps for hot deformation of α_2 aluminide alloy Ti-24Al-11Nb. *J. Mater. Sci.*, vol. 37, no. 6, pp. 1197-1201.

Narayana Murty, S. V. S.; Nageswara Rao, B.; Kashyap, B. P. (2003): On the hot working characteristics of 6061Al-SiC and 6061-Al_2O_3 particulate reinforced metal matrix composites. *Compos. Sci. Technol.*, vol. 63, no. 1, pp. 119-135.

Narayana Murty, S. V. S.; Nageswara Rao, B.; Kashyap, B. P. (2004): Development and validation of a processing map for AFNOR 7020 aluminium alloy. *Mater. Sci. Technol.*, vol. 20, no. 6, pp. 772-782.

Narayana Murty, S. V. S.; Nageswara Rao, B.; Kashyap, B. P. (2005a): Identification of flow instabilities in the processing maps of AISI 304 stainless steel. *J. Mater. Process. Technol.*, vol. 166, no. 2, pp. 268-278.

Narayana Murty, S. V. S.; Nageswara Rao, B.; Kashyap, B. P. (2005b): On the hot working characteristics of 2014 Al-20 vol%Al_2O_3metal matrix composite. *J. Mater. Process. Technol.*, vol. 166, no. 2, pp. 279-285.

Narayana Murty, S. V. S.; Torizuka, S.; Nagai, K. (2005): Microstructural evolution during simple heavy warm compression of a low carbon steel: Development of a processing map. *Mater. Sci. Eng. A*, vol. 410-411, pp. 319-323.

Picu, R. C.; Majorell, A. (2002): Mechanical behavior of Ti-6Al-4V at high and moderate temperatures-Part ¢ò: constitutive modelling. *Mater. Sci. Eng. A*, vol. 326, no. 2, pp. 306-316.

Polizzotto, C. (2008): Thermodynamics-based gradient plasticity theories with an application to interface models. *Int. J. Solids Struct.*, vol. 45, no. 17, pp. 4820-4834.

Prasad, Y. V. R. K.; Gegel, H. L.; Doraivelu, S. M.; Malas, J. C.; Morgan, J. T.; Lark, K. A.; Barker, D. R. (1984): Modeling of dynamic material behavior in hot deformation: Forging of Ti-6242. *Metall. Trans. A*, vol. 15, no. 10, pp. 1883-1892.

Prasad, Y. V. R. K.; Rao, K. P. (2005): Processing maps and rate controlling mechanisms of hot deformation of electrolytic tough pitch copper in the temperature range 300-950°. *Mater. Sci. Eng. A,* vol. 391, no. 1-2, pp. 141-150.

Prasad, Y. V. R. K.; Rao, K. P. (2006): Influence of oxygen on the processing maps for hot working of electrolytic tough pitch copper. *Mater. Lett.*, vol. 60, no. 21-22, pp. 2786-2790.

Prasad, Y. V. R. K.; Rao, K. P. (2008): Processing maps for hot deformation of rolled AZ31 magnesium alloy plate: Anisotropy of hot workability. *Mater. Sci. Eng. A*, vol. 487, no. 1-2, pp. 316-327.

Prasad, Y. V. R. K.; Rao, K. P.; Hort, N.; Kainer, K. U. (2008): Hot working parameters and mechanisms in as-cast Mg-3Sn-1Ca alloy. *Mater. Lett.*, vol. 62, no. 26, pp. 4207-4209.

Prasad, Y. V. R. K.; Sasidhara, S.; Sikka, V. K. (2000): Characterization of mechanisms of hot deformation of as-cast nickel aluminide alloy. *Intermetallics*, vol. 8, no. 9-11, pp. 987-995.

Prasad, Y. V. R. K.; Sastry, D. H.; Deevi, S. C. (2000): Processing maps for hot working of a P/M iron aluminide alloy. *Intermetallics*, vol. 8, no. 9-11, pp. 1067-1074.

Prasad, Y. V. R. K.; Sastry, D. H.; Deevi, S. C. (2001): Hot working behavior of extruded powder products of B2 iron aluminide alloys. *Mater. Sci. Eng. A*, vol. 311, no. 1-2, pp. 42-53.

Prasad, Y. V. R. K.; Seshacharyulu, T. (1998): Processing maps for hot working of titanium alloys. *Mater. Sci. Eng. A*, vol. 243, no. 1-2, pp. 82-88.

Raj, R. (1981): Development of a processing map for use in warm-forming and hot-forming processes. *Metall. Trans. A*, vol. 12, no. 6, pp. 1089-1097.

Rajagopal, K. R.; Srinivasa, A. R. (1998): Mechanics of the inelastic behavior of materials. Part ¢ò: inelastic response. *Int. J. Plasticity*, vol. 14, no. 10-11, pp. 969-995.

Rayleigh, L. (1873): On waves propagated along the plane surface of an elastic solid. *Proc. London Math. Soc.*, vol. 4, pp. 357-364.

Rayleigh, L. (1945): *Theory of Sound*, vol. 1. Dover Publications, New York.

Sagar, P. K. (2006): Effect of alloying elements and microstructure on the processing parameters of α_2 aluminide alloys. *Mater. Sci. Eng. A*, vol. 434, no. 1-2, pp. 259-268.

Semiatin, S. L. (1984): Fundamental definitions and workability tests used in flow localization studies, in: Semiatin, S.L., Jonas, J.J. (Eds), *Formability & Workability of Metals*. American Society of Metals, Ohio, pp. 13-23.

Semiatin, S. L.; Bieler, T. R. (2001): The effect of alpha platelet thickness on plastic flow during hot working of Ti-6Al-4V with a transformed microstructure. *Acta Mater.*, vol. 49, no. 17, pp. 3565-3573.

Semiatin, S. L.; Lahoti, G. D. (1981): Deformation and unstable flow in hot forging of Ti-6Al-2Sn-4Zr-2Mo-0.1Si. *Metall. Trans. A*, vol. 12, no. 10, pp. 1705-1717.

Semiatin, S. L.; Lahoti, G. D. (1982): The occurrence of shear bands in isothermal, hot forging. *Metall. Trans. A*, vol. 13, no. 2, pp. 275-288.

Seshacharyulu, T.; Medeiros, S. C.; Frazier, W. G.; Prasad, Y. V. R. K. (2000): Hot working of commercial Ti-6Al-4V with an equiaxed $\alpha - \beta$ microstructure: materials modeling considerations. *Mater. Sci. Eng. A*, vol. 284, no. 1-2, pp. 184-194.

Seshacharyulu, T.; Medeiros, S. C.; Frazier, W. G.; Prasad, Y. V. R. K. (2001): Unstable flow during supratransus working of Ti-6Al-4V. *Mater. Lett.*, vol. 47, no. 3, pp. 133-139.

Seshacharyulu, T.; Medeiros, S. C.; Frazier, W. G.; Prasad, Y. V. R. K. (2002): Microstructural mechanisms during hot working of commercial grade Ti-6Al-4V with lamellar starting structure. *Mater. Sci. Eng. A*, vol. 325, no. 1-2, pp. 112-125.

Seshacharyulu, T.; Medeiros, S. C.; Morgan, J. T.; Malas, J. C.; Frazier, W. G.; Prasad, Y. V. R. K. (2000): Hot deformation and microstructural damage mechanisms in extra-low interstitial grade Ti-6Al-4V. *Mater. Sci. Eng. A*, vol. 279,

no. 1-2, pp. 289-299.

Shaban, A.; Mahnken, R.; Wilke, L.; Potente, H.; Ridder, H. (2007): Simulation of rate dependent plasticity for polymers with asymmetric effects. *Int. J. Solids Struct.*, vol. 44, no. 18-19, pp. 6148-6162.

Thamburaja, P.; Ekambaram, R. (2007): Coupled thermo-mechanical modelling of bulk-metallic glasses: Theory, finite-element simulations and experimental verification. *J. Mech. Phys. Solids*, vol. 55, no. 6, pp. 1236-1273.

Varshni, Y. P. (1970): Temperature dependence of the elastic constants. *Phys. Rev. Sect. B*, vol. 2, pp. 3952-3958.

Voyiadjis, G. Z.; Abu Al-Rub, R. K. (2003): Thermodynamic based model for the evolution equation of the backstress in cyclic plasticity. *Int. J. Plasticity*, vol. 19, no. 12, pp. 2121-2147.

Voyiadjis, G. Z.; Abed, F. H. (2006): A coupled temperature and strain rate dependent yield function for dynamic deformations of bcc metals. *Int. J. Plasticity*, vol. 22, no. 8, pp. 1398-1431.

Voyiadjis, G. Z.; Deliktas, B. (2009): Formulation of strain gradient plasticity with interface energy in a consistent thermodynamic framework. *Int. J. Plasticity*, vol. 25, no. 10, pp. 1997-2024.

Zeng, W. D.; Shu, Y.; Zhang, X. M.; Zhou, Y. G.; Zhao, Y. Q.; Wu, H.; Dai, Y.; Yang, J.; Zhou, L. (2008): Hot workability and microstructure evolution of highly β stabilised Ti-25V-15Cr-0.3Si alloy. *Mater. Sci. Technol.*, vol. 24, no. 10, pp. 1222-1229.

Ziegler, H. (1963): *Progress in Solid Mechanics*, vol. 4. John Wiley and Sons, New York.

Zrník, J.; Kvackaj, T.; Pongpaybul, A.; Sricharoenchai, P.; Vilk, J.; Vrchovinsky, V. (2001): Effect of thermomechanical processing on the microstructure and mechanical properties of Nb-Ti microalloyed steel. *Mater. Sci. Eng. A*, vol. 319-321, pp. 321-325.